frontiers | Frontiers in Earth Science

TYPE Original Research
PUBLISHED 14 October 2022
DOI 10.3389/feart.2022.1014170

OPEN ACCESS

EDITED BY
Luigi Jovane,
University of São Paulo, Brazil

REVIEWED BY
Junhua Guo,
California State University, Bakersfield, United States
Hong Yeon Cho,
Korea Institute of Ocean Science and Technology (KIOST), South Korea

*CORRESPONDENCE
W. Ali,
w.ali@tudelft.nl

SPECIALTY SECTION
This article was submitted to Marine Geoscience, a section of the journal Frontiers in Earth Science

RECEIVED 08 August 2022
ACCEPTED 03 October 2022
PUBLISHED 14 October 2022

CITATION
Ali W, Enthoven D, Kirichek A, Chassagne C and Helmons R (2022), Effect of flocculation on turbidity currents.
Front. Earth Sci. 10:1014170.
doi: 10.3389/feart.2022.1014170

Effect of flocculation on turbidity currents

W. Ali[1]*, D. Enthoven[2], A. Kirichek[3], C. Chassagne[1] and R. Helmons[2,4]

[1]Section of Environmental Fluid Mechanics, Department of Hydraulic Engineering, Faculty of Civil Engineering and Geosciences, Delft University of Technology, Delft, Netherlands, [2]Section of Offshore and Dredging Engineering, Department of Maritime and Transport Engineering, Faculty of Mechanical, Maritime and Materials Engineering, Delft University of Technology, Delft, Netherlands, [3]Section of Rivers, Ports, Waterways and Dredging Engineering, Department of Hydraulic Engineering, Faculty of Civil Engineering and Geosciences, Delft University of Technology, Delft, Netherlands, [4]Section of Mineral Production and HSE, Department of Geoscience and Petroleum, Faculty of Engineering, Norwegian University of Science and Technology (NTNU), Trondheim, Norway

Flocculation between inorganic sediment, salt ions and microscopic organic matter present in the marine environment might play an important role in the dynamics of turbidity currents. The ability to predict, understand, and potentially leverage the effect of flocculation on turbidity currents will help to minimize the impact of human interventions such as dredging, trenching, and deep-sea mining. To better characterize the effect of flocculation on the benthic turbidity currents generated by these activities, a series of laboratory experiments were performed. Turbidity currents were created by means of lock exchange experiments. The present work focuses on the flocculation of clays that are representative for abyssal regions where deep-sea mining is performed, but most of the conclusions of this work are generic and can be applied to other types of benthic flows, occuring in harbours and channels. The effect of salt and organic material as flocculant agent was investigated. Various concentrations of clay and organic flocculant were tested. Video analysis was used to determine the head velocity of the plume. Samples at different run-out lengths were collected at the end of the lock exchange experiments for particle size and settling velocity measurements. The velocities of the turbidity currents in fresh and saline water (when no organic matter was present) were found to be similar, which was expected considering the timescales of salt-induced flocculation (about 30 min or more compared to the duration of lock exchange experiment <60 s). It was however demonstrated that, in presence of organic matter, flocculation occurred during the short time (30–60 s) of the experiment, leading to a reduced current propagation and a significant change in floc sizes (from 20 to 1,000 μm) and settling velocities (from 1 to 60 mm s^{-1}). Salt ions contributed to flocculation in the sense that flocculation with organic matter was improved in the presence of salt.

KEYWORDS

flocculation, deep sea mining, organic matter, cohesive sediment, dredging plume

1 Introduction

Dredging is commonly used for land reclamation, creating or deepening ports and waterways, and extracting minerals from underwater deposits. Over the last decade, the interest to the latter has substantially increased since the demand for minerals and metals has grown as the results of the World's population and economic activity surge. Dredging activities produce sediment plumes that lead to an increase in suspended solids concentration, potentially impacting benthic ecosystems. It is the most frequent causes of disturbance deep sea environments (Hobbs, 2002; Gates and Jones, 2012; Puig et al., 2012; Harris, 2014; Sharma, 2015). There is increasing interest in metals, particularly those critical for a successful renewable energy transition (e.g. wind turbines, solar panels and electric car storage batteries) (Hein et al., 2020). Precious metals such as manganese, nickel, cobalt are mined from terrestrial mining, however Deep Sea Mining (DSM) might be an alternative to fill the demand for precious metals. Polymetallic nodules, which contain significant amounts of these precious metals, are found in abundance on the abyssal plains in the deep sea. These nodules are distinguished from terrestrial deposits by the presence of many metals in a single deposit; for example, nodules from the Clarion–Clipperton Zone (CCZ) which is a large area with polymetallic nodules, contain cobalt, nickel, copper, and manganese in a single ore (Gillard, 2019; ISA, 2019; Harbour et al., 2020; Hein et al., 2020). In nodule mining, the Seafloor Mining Tool (SMT) collects nodules from the seafloor and separates them from excess water and fine sediments. The excess water and fine sediment are released behind the mining vehicle on the seafloor (Figure 1). There are four key areas of interest in the horizontal discharge of a sediment-water mixture from an SMT as shown in Figure 1 (Elerian et al., 2021).

1. Discharge source: This includes the preliminary conditions, including momentum, suspended sediment content, and z-distance from the sea bed. The SMT's design affects the physical parameters.

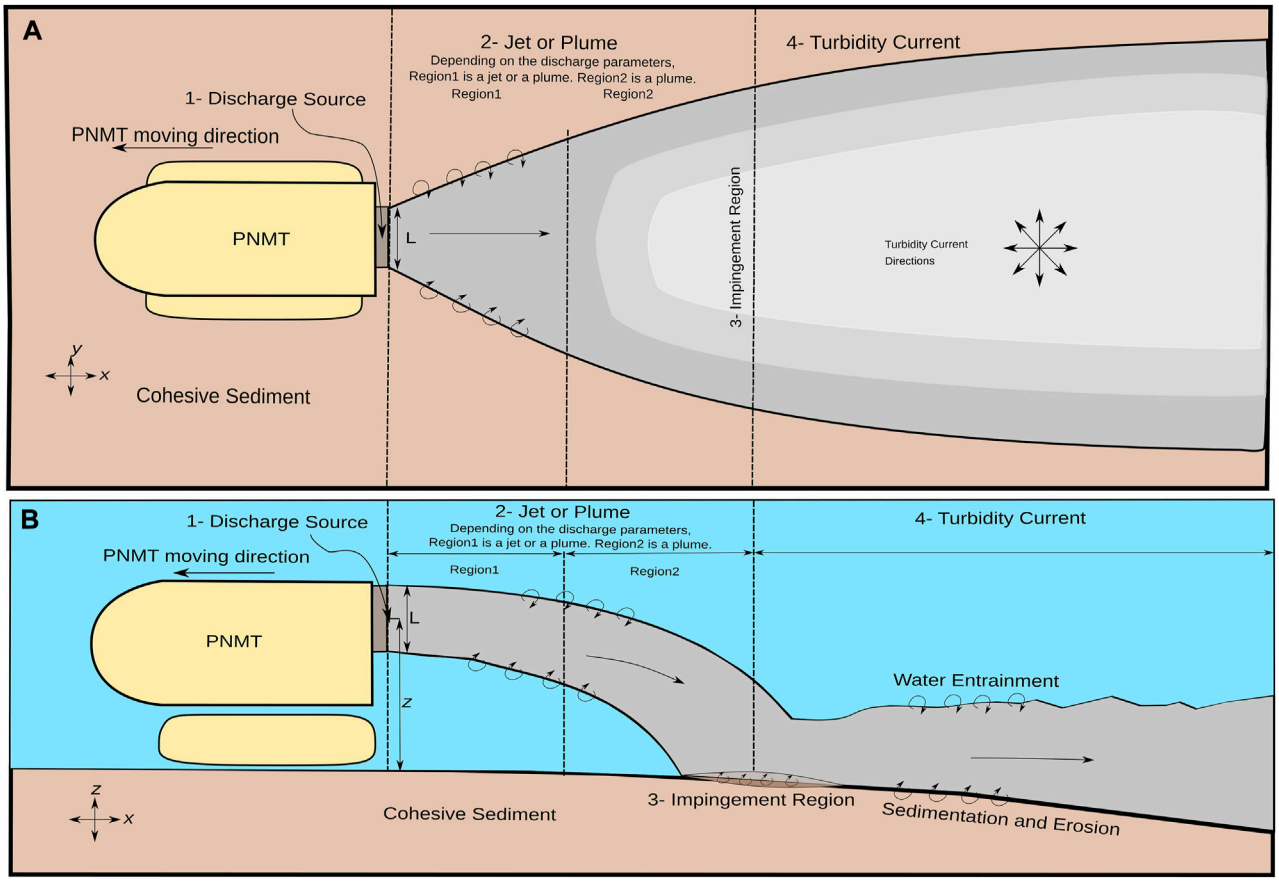

FIGURE 1
Schematic representation of how the sediment-water mixture discharged from a PNMT evolves (nearfield area). **(A)** Top view of the discharge process from a polymetallic nodule mining tool (PNMT) (Elerian et al., 2022) **(B)** Right-side view of the discharge process from a PNMT (Elerian et al., 2021).

TABLE 1 Mineral group percentages in deep-sea sediment: Inter Ocean Metal joint organization (IOM) data (Zawadzki et al., 2020), Global Sea Mineral Resources (GSR) data (Global Sea Mineral Resources, 2018), Sites A-C (Bisschof et al., 1979). It is worth noting that for IOM 1, 2, and 3, clay mineral percent is given relative to total sediment. Clay mineral percent is only relative to the sum of clay minerals at Sites A, B, C, and GSR.

	IOM 1	IOM 2	IOM 3	Site A	Site B	Site C	GSR	IOM
Smectite (%)	12.71	17.33	16.49	52	38	40	36.41	16.3
Illite (%)	13.82	12.05	14.52	31	42	50	48.34	13.2
Kaolinite (%)	0.65	0.43	0.54	17	20	10	10.33	1
Chlorite (%)	1.70	1.85	2.35				4.92	1.5
Amorphic (%)	50.47	47.09	44.42					

TABLE 2 Sediment fraction distribution: GSR and NTNU data (Lang et al., 2019), IOM data (Zawadzki et al., 2020). GSR provides averaged data based on the Belgium license area in the CCZ, while NTNU data is data of specific box-cores of the GSR data average. The IOM data is based on data from the CCZ's IOM license area.

Fraction	Diameter range (um)	GSR data average (%)	NTNU data BC062 (%)	NTNU data BC064 (%)	IOM data average (%)	Gillard et al. (2019)
Clay	<2	12.0	11.3	14.5	23.24	25.3
Silt	2–63	76.2	85.7	82.5	70.36	52.11
Sand	63–2000	11.8	3	3	6.13	22.5

2. Jet or Plume regime: Depending on the flow discharge parameters in this area, the flow may take the form of a jet or plume. Later, when buoyancy force takes over, the flow transforms into a plume.
3. Impingement region: This area is situated on the ocean floor. Due to the direct connection with the seafloor in this location, the negative buoyant plume changes direction. Within this region, sediment deposition and potential sea bed erosion are anticipated to occur.
4. Turbidity current: This current originates outside the area of impingement. The generated turbidity current's behavior is governed by the interaction between the discharge and the seabed (Rutkowska et al., 2014; Global Sea Mineral Resources, 2018; Hage et al., 2019; Ouillon et al., 2021). Its principal characteristics are determined by the hydraulic characteristics previous to the impingement region.

In the near-field region, many flow regimes (such as jet, plume, and turbidity current) are anticipated, and they rely on the discharge characteristics. The focus of this work is on turbidity current. It is estimated that the turbidity current generated from the discharge at the back of the mining vehicle can spread over large distances (9–13 km (Gillard, 2019)) and remain suspended for an extended period of time (Blue Nodules, 2020; Hein et al., 2020; Haalboom et al., 2022). The sediment plume generated by mining activity can severely affect the deep sea flora and fauna. The settling of the sediment plume and subsequent blanketing can bury benthic species, obstruct the respiratory surfaces of filter feeders, and contaminate the food source for the majority of benthic organisms (Vanreusel et al., 2016; Gollner et al., 2017; Jones et al., 2017). Limiting plume dispersion could help to lower the environmental impact caused by human activities (Weaver et al., 2022).

Particle size distribution (PSD) is an important factor that determines how far deep-sea sediment plumes spread (Gillard et al., 2019; Spearman et al., 2020). The coarse nodule debris settle quickly but the clay-sized mineral particles (Tables 1 and 2) stay in suspension for long periods of time which leads to a wider plume dispersion (Sharma, 2015). Since aggregated particles (flocs) settle quicker, flocculation has been shown to potentially limit plume dispersion (Manning and Dyer, 2002; Smith and Friedrichs, 2011; Gillard et al., 2019; Spearman et al., 2019, 2020). The size, density, shape, settling velocity and strength of flocs vary over time. These properties are influenced by the medium in which the particles are suspended (salinity, organic matter content, sediment concentration, hydrodynamics) (Manning and Dyer, 2002; Mietta et al., 2009; Smith and Friedrichs, 2011; Chassagne, 2020). The deep-sea environment is in principle favourable for flocculation because of its high salinity and concentration of organic matter (Mewes et al., 2014; ISA, 2015; Fettweis and Baeye, 2015; Volz et al., 2018). The availability of fresh organic matter on the top layer of the deep sea varies substantially because organic matter gradually degrades and remineralizes with depth. With increasing water depth, the flux of organic matter to the seabed often decreases. Less than 0.5 percent of the sediment bulk is made up of carbon in the top few centimeters of

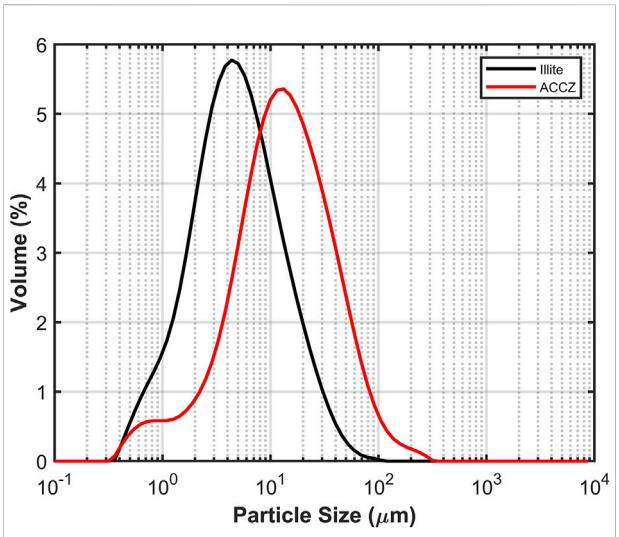

FIGURE 2
Particle size distribution of illite and ACCZ.

the CCZ sediment. This decreases to 0.1 percent of the sediment's mass below 30 cm (Volz et al., 2018). The present work aims to demonstrate the mechanisms that, in the presence of organic matter, can help reduce the extension of the turbidity currents. Flocculation has been shown to occur at very short timescales (in the order of few minutes) in natural environments in the presence of (microscopic) organic matter (Deng et al., 2019; Safar et al., 2019; Shakeel et al., 2020). The current lab-scale work uses a series of lock exchange experiments to generate a turbidity current and studies the impact of flocculation in short time scales. Properties such as time and distance of turbidity currents' propagation, particle size, and settling velocities are measured. This article is organized as follows. Section 2 gives an overview of the materials used and the experimental setups. Section 3 presents relevant results and discussion. Finally, the conclusions are presented in Section 4.

2 Material and methods

2.1 Clay

Two types of clays were used for the experiments. Initial experiments were conducted by using illite since illite is one of the dominant clay minerals (Table 2) found of the top layer of the Clarion–Clipperton Zone (CCZ) sediment where Deep Sea Mining (DSM) is performed (ISA, 2015; Helmons et al., 2022). The illite used in the experiments (purchased from Argiletz laboratoires) was obtained as a dry powder. The d_{50} of illite particles was found to be around 5 μm by static light scattering (Figure 2). A lab-made artificial clay with a composition similar to CCZ clay was also used and will be referred to as Artificial CCZ (ACCZ) (Enthoven, 2021; Ali et al., 2022). We use this material as a substitute for deep-sea sediment, as CCZ clay could not be supplied in sufficient quantities for lock-exchange experiments. The ACCZ mixture consists of two materials: i) Sibelco FT-S1 (Abidichte Ton) consisting of 64% kaolinite, 10% illite, 19% quartz, and 7% other minerals; ii) Cebo OMCA Betonite consisting of 17% kaolinite, 17% illite and 66% montmorillonite. The precise proportions of these two materials are unknown. The clay was created so that its rheological/mechanical properties match the ones of CCZ clay (Enthoven, 2021). The wet ACCZ clay was dried for 24 h at 105°C to determine its dry density, which was found to be 2,600 kg m^{-3}. This clay has an average particle size of 10–20 μm, as found by static light scattering device (Figure 2).

2.2 Flocculant

The organic matter found in the deep-sea region is expected to act as a flocculating agent for the sediment plume (Jones et al., 2017; Gillard et al., 2019; Spearman et al., 2020; Jones et al., 2021). It was impossible, at this stage, to fully characterize or obtain this flocculant, which is expected to be composed in parts of polyssacharides. As was done in previous studies (Shakeel et al., 2020), a synthetic flocculant was used as a proxy for organic matter content. The flocculant chosen was an anionic polyacrylamide, referenced Zetag 4,120 (BASF company) of medium anionic charge with high molecular weight. Polyelectrolytes with a high molecular weight will better promote flocculation compared to polyelectrolytes with a low molecular weight (Bergaya and Lagaly, 2013).

2.3 Lock exchange setup

Turbidity currents have been studied extensively in the laboratory through lock exchange experiments (Helena et al., 2013; Baker et al., 2017; Craig et al., 2020). Lock-exchange experiments or fixed volume turbidity currents are caused by the release of dense material in a fixed volume. The front propagation in a traditional lock-release turbidity current is equivalent to the front propagation in the turbidity current generated by a moving source (Ouillon et al., 2021).

Lock exchange experiments were performed in both fresh and saline water. The saline water was produced by mixing 10 mM of $CaCl_2$ to freshwater. The experiments were conducted for three distinct clay concentrations (10 g L^{-1}, 30 gL^{-1} and 100 g L^{-1}) with illite and two different concentrations with ACCZ (10 g L^{-1} and 30 g L^{-1}). Handling and mixing the higher concentration of ACCZ and eventually getting a fully dispersed sample was difficult therefore 100 g L^{-1} was not used. 30 g L^{-1} is the mean case, and 10 g L^{-1} and 100 g L^{-1} are considered to assess whether the design

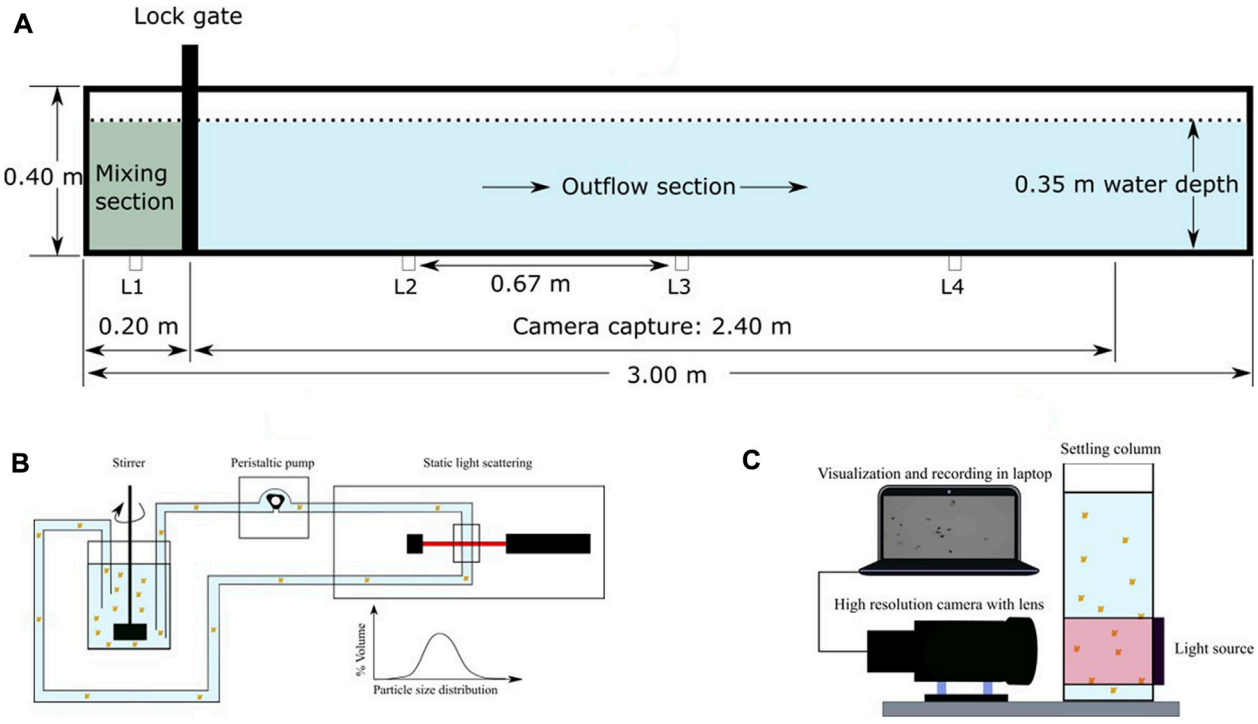

FIGURE 3
(A) Schematic representation of the Lock exchange setup. The samples are taken at L1, L2, L3 and L4 locations. **(B)** Schematic representation of the Malvern master Sizer 2000 for particle size measurement. **(C)** Schematic representation of the FLOCCAM setup.

should aim for lower or higher concentrations to identify if and when flocculation has a more significant effect (Blue Nodules, 2020). Two different flocculant dosages (0.25 mg g^{-1} and 0.75 mg g^{-1} of clay) were used for flocculation based on preliminary studies and are significantly below the optimum flocculant dosage (2.5 mg g^{-1}). The dry clay was mixed in water in the lock exchange's mixing section for an hour before the lock gate was opened. This mixing ensured that homogeneous suspensions with a well-defined mean particle size could be obtained. The initial clay size obtained by such a process might not be similar to that obtained through the DSM operation, in which the sediment passes through the SMT for a brief period of time exposed to high shear rates. In experiments with flocculant, the flocculant was added and stirred for 30 s before opening the lock. The turbidity flow was filmed with a Navitar 17 mm lens on an IL5HM8512D: Fastec high-speed camera. The camera was set 4.75 m from the lens to the front wall of the tank, and it recorded at a rate of 130 frames per second. The camera captured the 2.40 m to the left of the lock. Samples were collected from four locations (L1, L2, L3, L4 in Figure 3A) at the end of the experiments from the collection points located at the bottom of the lock exchange.

2.4 Particle/flocs size distribution

Particle Size Distribution (PSD) analysis was conducted on the obtained samples using a Malvern Master Sizer 2000 (Figure 3B), a technique based on static light scattering (SLS). With this set-up, within a few seconds a full PSD can be recorded. The measurements were carried out in a JLT6 jar setup supplied by VELP Scientifica, Italy. The size of the jar was 95 mm in diameter and 110 mm in height. The suspension was stirred using a single rectangular paddle. The paddle was 25 mm in height and 75 mm in diameter and was positioned in the suspension 10 mm above the bottom of the jar. The suspension was pumped through the Malvern Master Sizer 2000 from the mixing jar to the Mastersizer and then back to the mixing jar using a peristaltic pump (Figure 3B). The lowest possible discharge rate of the pump was used (1.37 ml s^{-1} (112 s^{-1})).

2.5 Floc settling analysis

The FLOCCAM device is based on video microscopy and can be used to estimate PSD's (>20 μm) and settling velocities of flocs samples (Shakeel et al., 2021; Ye et al., 2020; Manning et al., 2007;

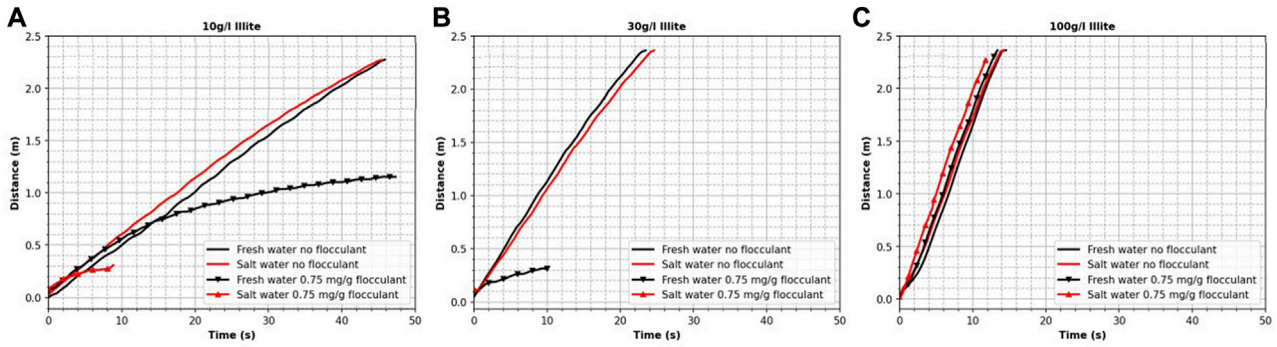

FIGURE 4
Change in distance as a function of time for 10 g L^{-1} **(A)**, 30 g L^{-1} **(B)** and 100 g L^{-1} **(C)** of illite. Black lines represent experiments done in freshwater and red lines show experiments done in saltwater. Only results with 0.75 mg g^{-1} of flocculant are shown in these figures.

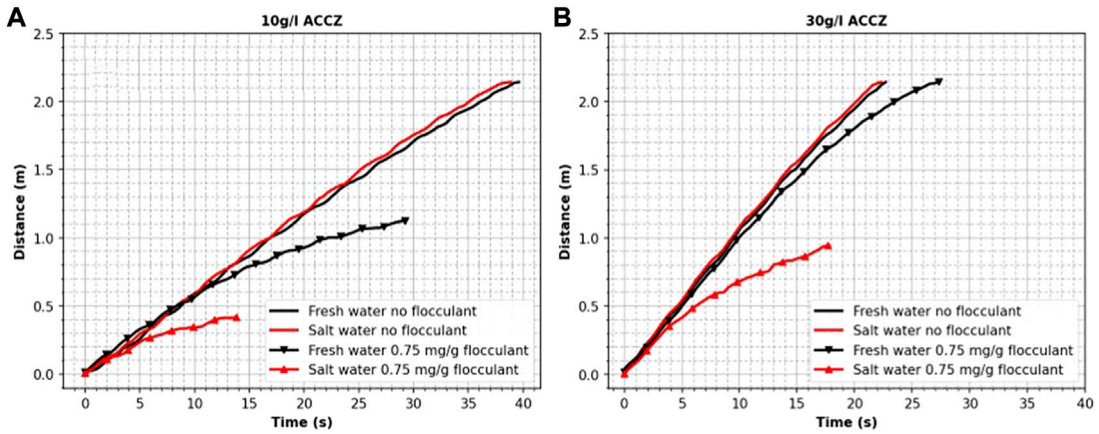

FIGURE 5
Change in distance as a function of time for 10 g L^{-1} **(A)** and 30 g L^{-1} **(B)** of ACCZ (Ali et al., 2022). Black lines represent experiments done in freshwater and red lines show experiments done in saltwater. Only results with 0.75 mg g^{-1} of flocculant are shown in these figures.

Mietta et al., 2009). Figure 3C shows a schematic representation of the equipment. The PSD, shape, and settling velocity of the flocs are calculated from recorded videos of settling flocs in a settling column using a software package called Safas (MacIver, 2019).

3 Results and discussion

3.1 Distance travelled by plume heads

The 10, 30, and 100 g L^{-1} illite experiments are displayed in Figure 4 in terms of the distance traveled by the turbidity current within the video recording range. When no flocculant is used, there is no significant difference observed between experiments conducted in fresh and saltwater and the turbidity current without added flocculant reached the lock exchange's end in all experiments. The current's head velocity scales as the square root of the plume density, as is expected (Huppert, 2006). Salt induced flocculation time is in the order of 15–30 min even under ideal shear circumstances (Mietta, 2010). Therefore, no significant effect was observed over the experimental period of the current study (<1 min). Similar results were obtained for both 10 and 30 g L^{-1} experiments done with ACCZ (see Figure 5).

Due to the effect of flocculation, the distance traveled in saltwater experiments with flocculant for all clay concentrations was reduced considerably. Figures 4, 5 show results for the experiments 0.75 mg/g flocculant where the sediment plume did not reach the lock exchange's endpoint and settled inside

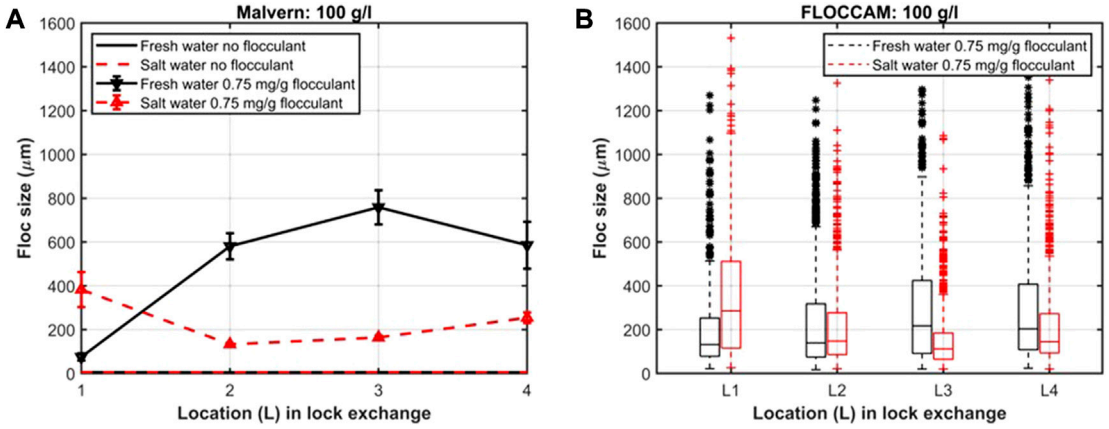

FIGURE 6
Hydrodynamic diameter of illite flocs for 100 g L^{-1} experiments at L1-L4 locations of the lock exchange. Figure **(A)**, results obtained by SLS and figure **(B)**, results obtained from FLOCCAM. Black and red lines represent experiments done in freshwater and saltwater, respectively. Only results with 0.75 mg g^{-1} of flocculant are shown.

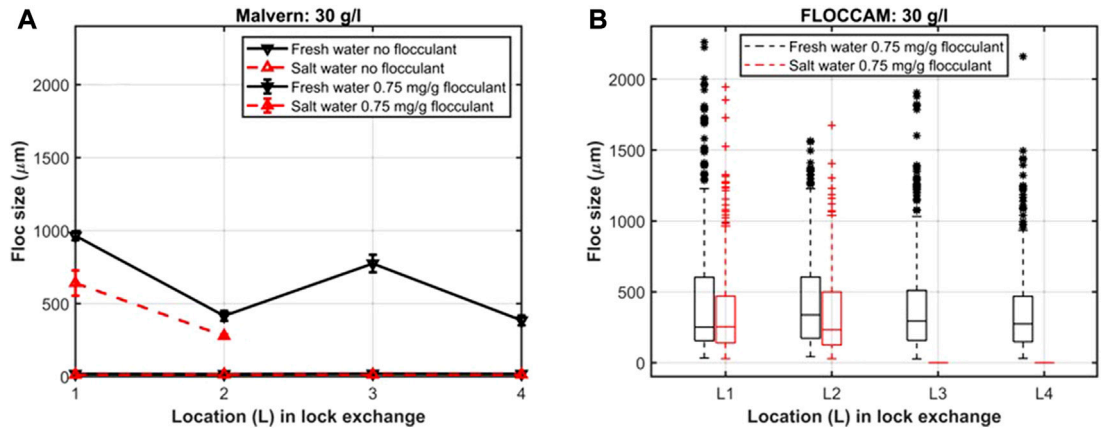

FIGURE 7
Hydrodynamic diameter of ACCZ flocs for 30 g L^{-1} experiments at L1-L4 locations of the lock exchange (Ali et al., 2022). Figure **(A)**, results obtained by SLS and figure **(B)**, results obtained from FLOCCAM. Black and red lines represent experiments done in freshwater and saltwater, respectively. Only results with 0.75 mg g^{-1} of flocculant are shown.

the outflow section. For the experiment done in freshwater with flocculant, the sediment plume reached the end of the outflow section or nearly half of the outflow section. The weak flocculation in freshwater accounts for this difference between fresh and saline water experiments. Even though both clay and flocculant have a negative charge, making flocculation difficult, freshwater contains enough cations to promote flocculation (Ibanez Sanz, 2018). The cation concentration in saltwater promotes flocculation, especially as the cation chosen (Ca^{2+}) is divalent (Shakeel et al., 2020; Chassagne, 2020). For 100 g L^{-1} experiment with illite, it is observed that the system did not properly flocculate as in all cases the sediment plume reached the end of the outflow section with the same speed, and flocculation had little to no effect on macroscopic scale.

The results using 0.25 mg g^{-1} flocculant are given in (Supplementary Figures S1, S2), and in all cases (illite or ACCZ), the sediment plume reached the end of outflow section except for one case (10 g L^{-1} ACCZ in saltwater). The results in the 0.25 mg g^{-1} case hint that the low concentration of flocculant has less impact on the plume propagation.

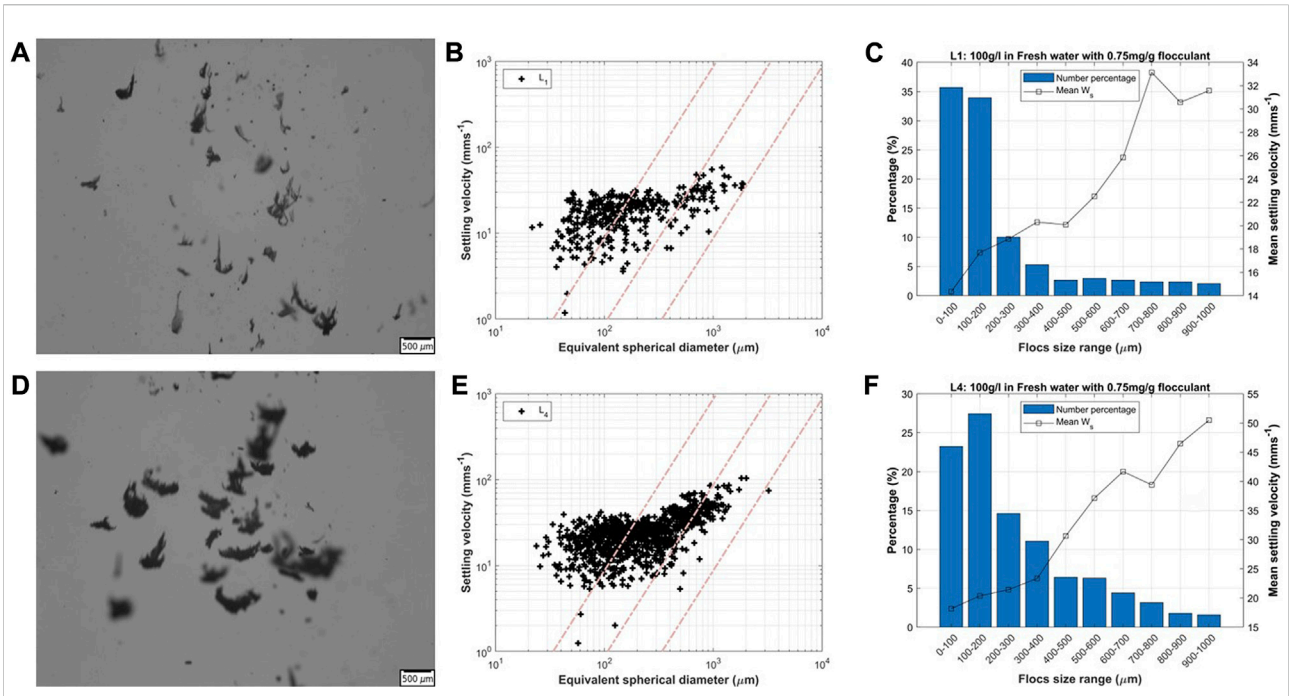

FIGURE 8
Figures **(A,D)** snapshots of the videos; Figures **(B,E)**: Settling velocity and particle size analysis of the samples collected at location L1 and L4 during lock exchange experiments with 100 g L^{-1} illite and 0.75 mg g^{-1} of flocculant in freshwater. Settling velocity is derived as a function of equivalent spherical diameter, with diagonal dashed lines representing the contours of effective density calculated by using Stokes equation (from left to right: 1600, 160, 16 (kg m^{-3})). Figures **(C,F)** show floc size range and mean settling velocity.

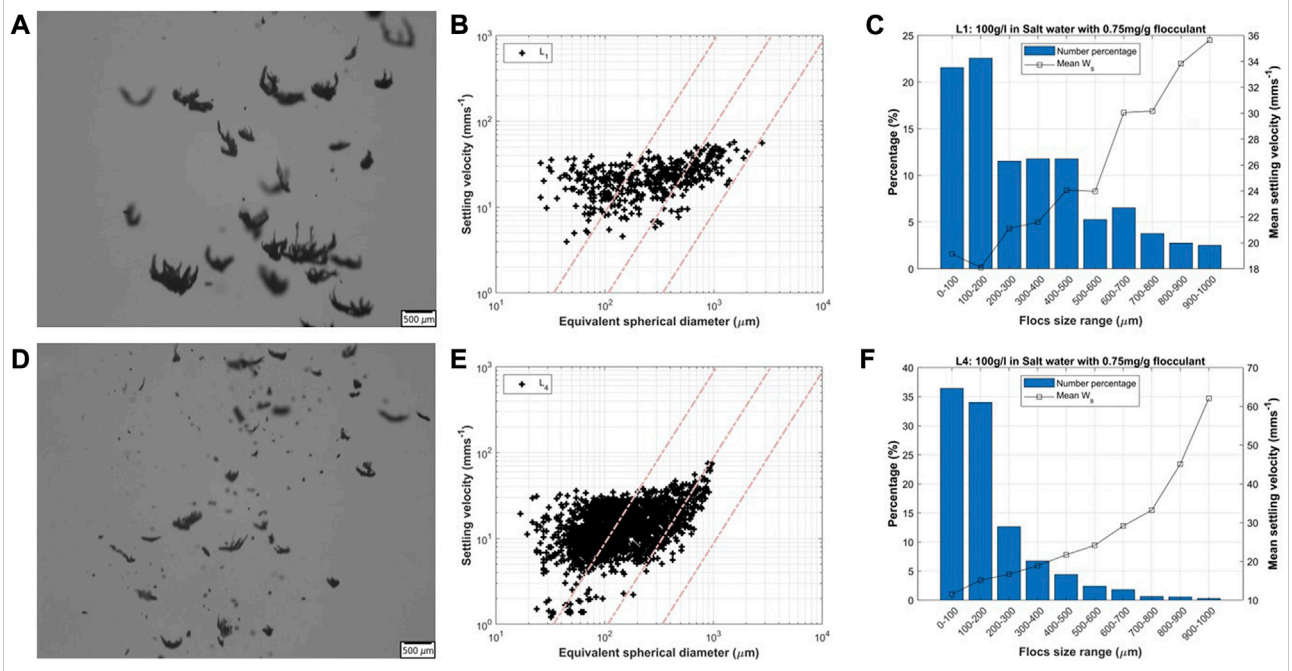

FIGURE 9
Figures **(A,D)** snapshots of the videos; Figures **(B,E)**: Settling velocity and particle size analysis of the samples collected at location L1 and L4 during lock exchange experiments with 100 g L^{-1} illite and 0.75 mg g^{-1} of flocculant in saltwater. Settling velocity is derived as a function of equivalent spherical diameter, with diagonal dashed lines representing the contours of effective density calculated by using Stokes equation (from left to right: 1600, 160, 16 (kg m^{-3})). Figures **(C,F)** show floc size range and mean settling velocity.

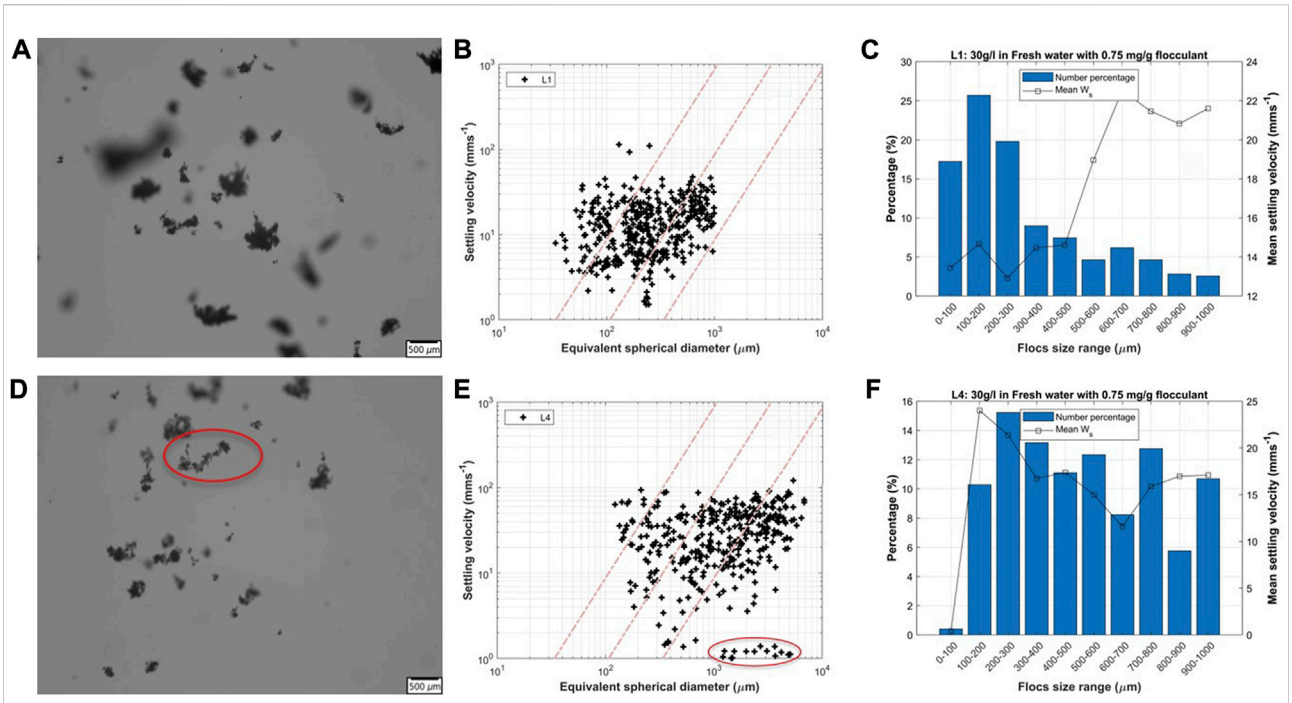

FIGURE 10
Figures **(A,D)** snapshots of the videos; Figures **(B,E)**: Settling velocity and particle size analysis of the samples collected at location L1 and L4 during lock exchange experiments with 30 g L^{-1} ACCZ and 0.75 mg g^{-1} of flocculant in freshwater (Ali et al., 2022). Settling velocity is derived as a function of equivalent spherical diameter, with diagonal dashed lines representing the contours of effective density calculated by using Stokes equation (from left to right: 1600, 160, 16 (kg m^{-3})). Figures **(C,F)** show floc size range and mean settling velocity.

3.2 Mean floc size as function of travel distance

Figure 6 (Illite) and Figure 7ACCZ show the mean floc size of the samples taken at locations L1–L4. No flocculation occurred without the flocculant in both fresh and saltwater, as for each location, the d_{50} was found equal to the mean clay size. For both experiments with illite, d_{50} was found to be around 5 μm at all locations, whereas for experiment with ACCZ, it was found to be between 12 and 20 μm. These sizes are in line with the d_{50} found by SLS (5 and 10–20 μm respectively, see section 2.1). The bars given in Figure 6 and Figure 7A represent the standard deviation around the mean floc size based on SLS device, whereas the box plots in Figure 6 and Figure 7B represent the median particle sizes with interquartile range and outliers based on FLOCCAM. In the presence of flocculant, it was found that freshwater flocs were larger than saltwater flocs. Because of the electrostatic repulsion between the charged groups on the polymeric flocculant backbones, the flocculant in freshwater is less coiled in fresh than in salt water (Chassagne, 2020). As a result of shear during propagation, it is observed that the d_{50} of flocs created in saltwater with illite clay reduced as function of travel distance. This difference is not observed for the ACCZ clay (Figure 6 and Figure 7).

The results obtained with 0.25 mg g^{-1} flocculant are shown in (Supplementary Figures S3, S4), where the difference in flocs size in fresh and salt water is not significant.

3.3 Settling velocity distributions as function of size and travel distance

Figures 8, 9 show the settling velocities and particle size for 100 g L^{-1} illite with 0.75 mg g^{-1} flocculant at L1 and L4 for freshwater and saltwater, respectively. Figures 10, 11 show the settling velocities and particle size for 30 g L^{-1} ACCZ with 0.75 mg g^{-1} of flocculant at sites L1 and L4 (for freshwater) and L1 and L2 (for saltwater), respectively. At the point when the turbidity current settles down, on average the settling velocities in freshwater are smaller than in saltwater. This is due to the fact that the flocculant is less coiled in freshwater than in saltwater (Chassagne, 2020), where flocs are denser and have a faster settling velocity. This was confirmed by the video images (see Figure 8 and Figures 9A,D). The settling velocities increased in the case of saltwater for 100 g L^{-1} illite between L1 and L4, as a result of coiling, flocs got compacted right after opening the lock (Figure 9). In the case of 30 g L^{-1} ACCZ, the settling behavior and floc size for the saltwater sample did not change between L1 and L2, indicating that

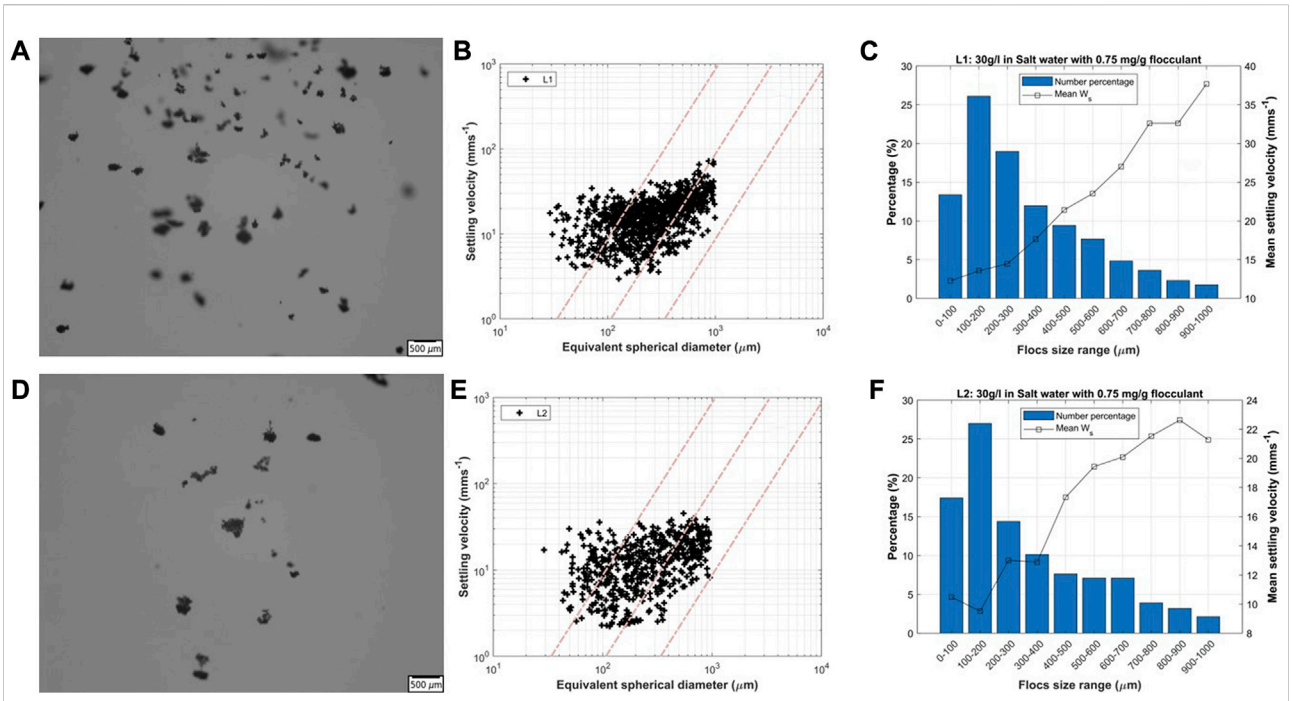

FIGURE 11
Figures **(A,D)** snapshots of the videos; Figures **(B,E)**: Settling velocity and particle size analysis of the samples collected at location L1 and L2 during lock exchange experiments with 30 g L^{-1} ACCZ and 0.75 mg g^{-1} of flocculant in saltwater (Ali et al., 2022). Settling velocity is derived as a function of equivalent spherical diameter, with diagonal dashed lines representing the contours of effective density calculated by using Stokes equation (from left to right: 1600, 160, 16 (kg m^{-3})). Figures **(C,F)** show floc size range and mean settling velocity.

optimum flocculation (i.e. flocs cannot grow any further) has occurred in the mixing tank. The bridging between anionic polyelectrolyte and clay is complete because of saltwater cations. The flocculation in the mixing tank for the freshwater sample is most likely incomplete due to the scarcity of cations. Flocs, clay particles, and unbounded flocculant are released when the lock is opened. Freshwater containing cations comes into contact with the clay particles and unbounded flocculant. Because polyelectrolyte flocculation is quick (on the scale of seconds) (Ibanez Sanz, 2018; Shakeel et al., 2020; Ali and Chassagne, 2022), these cations can act as a binding agent, inducing flocculation. As a result, flocs form, resulting in a particle size change, as shown between L1 and L4. Several flocs formed during the propagation of the sediment plume in 30 g L^{-1} ACCZ experiment in freshwater are observed to be elongated, resulting in flocs with larger equivalent diameters (shown by the red circle in Figure 10D). Because they are formed of low density uncoiled flocculant with some clay linked to it, these big flocs have a very slow settling velocity. These flocs were unable to catch more clay particles and coil due to their limited residence period in the water column. Coiling of flocs happens over longer periods of time when turbulent shear causes the polyelectrolyte's dangling ends to fall onto the floc. The flocs get rounder and denser as a result (Shakeel et al., 2020). Our experiments show that the amount of flocculant needed correlates to clay concentration. In addition, the results obtained with 30 g L^{-1} with 0.75 mg g^{-1} combination results in a turbidity current that settles faster than other combinations. The results with 0.25 mg g^{-1} of flocculant are shown in Supplementary Figures S5-S8.

4 Conclusion

Understanding the changes in the propagation of turbidity currents created by human interventions, such as dredging, trenching and deep-sea mining is crucial for anticipating, predicting and where possible reducing the related environmental impact. Understanding is also crucial for engineers to know in what way the equipment and processes could be optimized to minimize plume dispersion. Previous studies have demonstrated that the flocculation of organic matter to clay occurs in less than 1 min in series of laboratory experiments. In this work, the influence of flocculation on turbidity currents was studied inside a lock exchange, where the current propagation time was of the same order of magnitude. It was shown that in the presence of an organic flocculating agent (anionic polyelectrolyte) flocculation was promoted. It was found

that in both fresh and saltwater, flocs can be formed in a matter of seconds with the flocculant used in this study. As a result, the sediment plume was able to settle more quickly. The synthetic flocculant used is a proxy for organic matter found in marine environments (usually also negatively charged). It remains to be investigated if the type of flocculant has a significant impact on flocculation. This will be possible once the organic matter found in our area of interest (i.e. the Clarion-Clipperton Zone) has been fully characterized. The results presented in this article are generic, thus apply to a wide range of turbidity currents. We demonstrated that flocculation may occur even in freshwater, where flocculation is supposed to be difficult because of the electrostatic repulsion between organic matter and clay. This means that flocculation should be accounted for in turbidity current models. The obtained results demonstrate that flocculation is a relevant phenomenon that may already be contributing in the near field. Building experience with more conventional sediments allows us to better understand and design experiments with real CCZ sediment, which is the next step.

Data availability statement

The original contributions presented in the study are included in the article/Supplementary Material, further inquiries can be directed to the corresponding author.

Author contributions

WA first draft manuscript and floc experiments. DE and WA lock exchange experiments, AK, CC, and RH contributed to data analysis and interpretation. All authors contributed to the manuscript's revision and read and approved the submitted version.

Funding

This work is performed in the framework of PlumeFloc (TMW.BL.019.004, Topsector Water and Maritiem: Blauwe route) within the MUDNET academic network.

Acknowledgments

The authors would like to thank all co-funding partners. The authors would also like to thank Deltares for using their experimental facilities in the framework of the MoU between TU Delft/Deltares.

Conflict of interest

The authors declare that the research was conducted in the absence of any commercial or financial relationships that could be construed as a potential conflict of interest.

Publisher's note

Supplementary material

The Supplementary Material for this article can be found online at: https://www.frontiersin.org/articles/10.3389/feart.2022.1014170/full#supplementary-material

References

Ali, W., and Chassagne, C. (2022). *Comparison between two analytical models to study the flocculation of mineral clay by polyelectrolytes*.

Ali, W., Enthoven, D., Kirichek, A., Helmons, R., and Chassagne, C. (2022). "Can flocculation reduce the dispersion of deep sea sediment plumes?" in Proceedings of the World dredging conference, Copenhagen, Denmark.

Baker, M. L., Baas, J. H., Malarkey, J., Jacinto, R. S., Craig, M. J., Kane, I. A., et al. (2017). The effect of clay type on the properties of cohesive sediment gravity flows and their deposits. *J. Sediment. Res.* 87 (11), 1176–1195. doi:10.2110/jsr.2017.63

Bergaya, F., and Lagaly, G. (2013). *Handbook of clay science*. Second edition. Amsterdam: Elsevier.

Bisschof, J., Heath, G., and Leinen, M. (1979). "Geochemistry of deep-sea sediments from the pacific manganese nodule province DOMES sites A, B and C," in *Marine geology and oceanography of the pacific manganese nodule province, marine science*. Editors J. Bisschof and D. Piper (Boston: Springer), 397–436.

Blue Nodules (2020). *Environmental Impact Assessment (EIA) components for test mining up to prototype level (TRL 6) Technical report*.

Chassagne, C. (2020). *Introduction to colloid science*. Delft Academic Press.

Craig, M. J., Baas, J. H., Amos, K. J., Strachan, L. J., Manning, A. J., Paterson, D. M., et al. (2020). Biomediation of submarine sediment gravity flow dynamics. *Geology* 48 (1), 72–76. doi:10.1130/G46837.1

Deng, Z., He, Q., Safar, Z., and Chassagne, C. (2019). The role of algae in fine sediment flocculation: *In-situ* and laboratory measurements. *Mar. Geol.* 71–84, 71–84. doi:10.1016/j.margeo.2019.02.003

Elerian, M., Alhaddad, S., Helmons, R., and van Rhee, C. (2021). Near-field analysis of turbidity flows generated by polymetallic nodule mining tools. *Mining* 1, 251–278. doi:10.3390/mining1030017

Elerian, M., Van Rhee, C., and Helmons, R. (2022). Experimental and numerical modelling of deep-sea-Mining-Generated turbidity currents. *Minerals* 12 (5), 558. doi:10.3390/min12050558

Enthoven, D. (2021). "Plume dispersion of low-density clayey suspension turbidity currents created by deep-sea mining," (Technische Universiteit Delft). Master Thesis.

Fettweis, M., and Baeye, M. (2015). Seasonal variation in concentration, size, and settling velocity of muddy marine flocs in the benthic boundary layer. *J. Geophys. Res. Oceans* 120, 5648–5667. doi:10.1002/2014jc010644

Gates, A. R., and Jones, D. O. B. (2012). Recovery of benthic megafauna from anthropogenic disturbance at a hydrocarbon drilling well (380 m depth in the Norwegian Sea). *PLoS ONE* 7, e44114. doi:10.1371/journal.pone.0044114

Gillard, B., Purkiani, K., Chatzievangelou, D., Vink, A., Iversen, M. H., and Thomsen, L. (2019). Physical and hydrodynamic properties of deep sea mining-generated, abyssal sediment plumes in the Clarion Clipperton Fracture Zone (eastern-central Pacific). *Elem. Sci. Anthropocene* 7, 5. doi:10.1525/elementa.343

Gillard, B. (2019). "Towards deep sea mining-impact of mining activities on benthic pelagic coupling in the clarion clipperton fracture Zone," (Universität Bremen). PhD Thesis.

Global Sea Mineral Resources (2018). *Environmental Impact Statement Small-scale testing of nodule collector components on the seafloor of the Clarion-Clipperton Fracture Zone and its environmental impact*.

Gollner, S., Kaiser, S., Menzel, L., Jones, D. O. B., Brown, A., Mestre, N. C., et al. (2017). Resilience of benthic deep-sea fauna tomining activities. *Mar. Environ. Res.* 129, 76–101. doi:10.1016/j.marenvres.2017.04.010

Haalboom, S., Schoening, T., Urban, P., Gazis, I. Z., de Stigter, H., Gillard, B., et al. (2022). Monitoring of anthropogenic sediment plumes in the clarion-clipperton Zone, NE equatorial pacific ocean. *Front. Mar. Sci.* 9. doi:10.3389/fmars.2022.882155

Hage, S., Cartigny, M., Sumner, E. J., Clare, M. A., Hughes Clarke, J. E., Talling, P. J., et al. (2019). Direct monitoring reveals initiation of turbidity currents from extremely dilute river plumes. *Geophys. Res. Lett.* 46 (20), 11310–11320. doi:10.1029/2019GL084526

Harbour, P. R., Leitner, A. B., Ruehlemann, C., Annemiek, V., and Sweetman, A. K. (2020). Benthic and demersal scavenger biodiversity in the eastern end of the clarion-clipperton Zone – an area marked for polymetallic nodule mining. *Front. Mar. Sci.* 1–14. doi:10.3389/fmars.2020.00458

Harris, P. T. (2014). Shelf and deep-sea sedimentary environments and physical benthic disturbance regimes: A review and synthesis. *Mar. Geol.* 353, 169–184. doi:10.1016/j.margeo.2014.03.023

Hein, J. R., Koschinsky, A., and Kuhn, T. (2020). Deep-ocean polymetallic nodules as a resource for critical materials. *Nat. Rev. Earth Environ.* 1 (3), 158–169. doi:10.1038/s43017-020-0027-0

Helena, N., Adduce, C., Alves, E., and Franca, M. (2013). Analysis of lock exchange gravity currents over smooth and rough beds. *J. Hydraulic Res.* 51 (4), 417–431. doi:10.1080/00221686.2013.798363

Helmons, R., de Wit, L., de Stigter, H., and Spearman, J. (2022). Dispersion of benthic plumes in deep-sea mining: What lessons can Be learned from dredging? *Front. Earth Sci.* 10, 868701. doi:10.3389/feart.2022.868701

Hobbs, C. H., III (2002). An investigation of potential consequences of marine mining in shallow water: An example from the mid-atlantic coast of the United States. *J. Coast. Res.* 18, 94–101.

Huppert, H. (2006). Gravity currents: A personal perspective. *J. Fluid Mech.* 554, 299–322. doi:10.1017/S002211200600930X

Ibanez Sanz, M. (2018). "Flocculation and consolidation of cohesive sediments under the influence of coagulant and flocculant," (Delft University of Technology). PhD Thesis.

ISA (2015). *A geological model of polymetallic nodule deposits in the clarion-clipperton fracture Zone*.

ISA (2019). *Current status of the reserved areas with the international seabed authority*.

Jones, D. O. B., Kaiser, S., Sweetman, A. K., Smith, C. R., Menot, L., Vink, A., et al. (2017). Biological responses to disturbance from simulated deep-sea polymetallic nodule mining. *PLOS ONE* 12 (2), e0171750. doi:10.1371/journal.pone.0171750

Jones, D. O. B., Simon-Lledó, E., Amon, D. J., Bett, B. J., Caulle, C., Clément, L., et al. (2021). Environment, ecology, and potential effectiveness of an area protected from deep-sea mining (Clarion Clipperton Zone, abyssal Pacific). *Prog. Oceanogr.* 197, 102653. doi:10.1016/j.pocean.2021.102653

Lang, A., Dasselaar, S., Aasly, K., and Larsen, E. (2019). *Blue nodules deliverable report D3.4: Report describing the process flow overview*.

MacIver, M. R. (2019). Safas: Sedimentation and floc analysis software. Available at https://github.com/rmaciver/safas.

Manning, A., Friend, P., Prowse, N., and Amos, C. (2007). Estuarine mud flocculation properties determined using an annular mini-flume and the LabSFLOC system. *Cont. Shelf Res.* 27 (8), 1080–1095. doi:10.1016/j.csr.2006.04.011

Manning, A. J., and Dyer, K. R. (2002). A comparison of floc properties observed during neap and spring tidal. *Proc. Mar. Sci.*, 233–250.

Mewes, K., Mogollón, J. M., Picard, A., Rühlemann, C., Kuhn, T., Nöthen, K., et al. (2014). Impact of depositional and biogeochemical processes on small scale variations in nodule abundance in the Clarion-Clipperton Fracture Zone. *Deep Sea Res. Part I Oceanogr. Res. Pap.* 91, 125–141. doi:10.1016/j.dsr.2014.06.001

Mietta, F., Chassagne, C., Manning, A. J., and Winterwerp, J. C. (2009). In-fluence of shear rate, organic matter content, pH and salinity on mud flocculation. *Ocean. Dyn.* 59 (5), 751–763. doi:10.1007/s10236-009-0231-4

Mietta, F. (2010). "Evolution of the floc size distribution of cohesive sediments," (Delft University of Technology). PhD Thesis.

Ouillon, R., Kakoutas, C., Meiburg, E., and Peacock, T. (2021). Gravity currents from moving sources. *J. Fluid Mech.* 924, A43. doi:10.1017/jfm.2021.654

Puig, P., Canals, M., Company, J. B., Martı'n, J., Amblas, D., Lastras, G., et al. (2012). Ploughing the deep sea floor. *Nature* 489, 286–289. doi:10.1038/nature11410

Rutkowska, M., Dubalska, K., Bajger-Nowak, G., Konieczka, P., and Namieśnik, J. (2014). Organomercury compounds in environmental samples: Emission sources, toxicity, environmental fate, and determination. *Crit. Rev. Environ. Sci. Technol.* 44, 638–704. doi:10.1080/10643389.2012.728825

Safar, Z., Rijnsburger, S., Sanz, M. I., Chassagne, C., Manning, A., Pietrzak, J., et al. (2019). "Characterization and dynamics of suspended particulate matter in the near field of the rhine river plume during a neap tide," in *Geophysical research abstracts*, 21.

Shakeel, A., MacIver, M. R., van Kan, P. J. M., Kirichek, A., and Chassagne, C. (2021). A rheological and microstructural study of two-step yielding in mud samples from a port area. *Colloids Surfaces A Physicochem. Eng. Aspects* 624, 126827. doi:10.1016/j.colsurfa.2021.126827

Shakeel, A., Safar, Z., Ibanez, M., Paassen, L., and Chassagne, C. (2020). Flocculation of clay suspensions by anionic and cationic polyelectrolytes a systematic analysis. *Minerals* 10, 999–1024. doi:10.3390/min10110999

Sharma, R. (2015). Environmental issues of deep-sea mining. *Procedia Earth Planet. Sci.* 11, 204–211. doi:10.1016/j.proeps.2015.06.026

Smith, S. J., and Friedrichs, C. T. (2011). Size and settling velocities of cohesive flocs and suspended sediment aggregates in a trailing suction hopper dredge plume. *Cont. Shelf Res.* 31 (10), S50–S63. doi:10.1016/j.csr.2010.04.002

Spearman, J., Taylor, J., Crossouard, N., Cooper, A., Turnbull, M., Manning, A., et al. (2020). Measurement and modelling of deep sea sediment plumes and implications for deep sea mining. *Sci. Rep.* 10 (1), 5075–5114. doi:10.1038/s41598-020-61837-y

Spearman, J., Taylor, J., Crossouard, N., Cooper, A., Turnbull, M., Manning, A., et al. (2019). "The measurement and modelling of plumes resulting from deep sea mining of Fe-Mn Crusts," in Proceedings of the World dredging conference (WODCONXXII), Shanghai, China.

Vanreusel, A., Hilario, A., Ribeiro, P. A., and Menot, L. (2016). *Threatened by mining, polymetallic nodules are required to preserve abyssal epifauna*. Nature Publishing Group, 1–6.

Volz, J. B., Mogollon, J. M., Geibert, W., Arbizu, P. M., Koschinsky, A., and Kasten, S. (2018). Natural spatial variability of depositional conditions, biogeochemical processes and element fluxes in sediments of the eastern Clarion Clipperton Zone, Pacific Ocean. *Deep Sea Res. Part I Oceanogr. Res. Pap.* 140, 159–172. doi:10.1016/j.dsr.2018.08.006

Weaver, P. P. E., Aguzzi, J., Boschen-Rose, R. E., Colaço, A., de Stigter, H., Gollner, S., et al. (2022). Assessing plume impacts caused by polymetallic nodule mining vehicles. *Mar. Policy* 139, 105011. doi:10.1016/j.marpol.2022.105011

Ye, L., Manning, A. J., and Hsu, T. J. (2020). Corrigendum to ``Oil-mineral flocculation and settling velocity in saline water''. *Water Res.* 173, 116180. doi:10.1016/j.watres.2020.116180

Zawadzki, D., Maciag, L., Abramowski, T., and McCartney, K. (2020). Fractionation trends and variability of rare Earth elements and selected critical metals in pelagic sediment from abyssal basin of NE pacific (Clarion-Clipperton fracture Zone). *Minerals* 10, 320. doi:10.3390/min10040320